

Creep Analysis of the FGM Cylinder under Steady-state Symmetric Loading

N. Habibi^{a,*}, S. Samawati^b, O. Ahmadi^c

^{a,*}Mechanical Engineering Department, University of Kurdistan, Iran.

^bMechanical Engineering Department, Khajeh Nasir Toosi University of Technology, Iran.

^cMechanical Engineering Department, Urmia University, Iran.

Article info

Article history:

Received 2016.04.26

Received in revised form
2016.07.01

Accepted 2016.07.19

Keywords:

Exact Solution
Rotary Cylinder
Creep
Navier Equation

Abstract

In this paper, a semi-analytical method for creep investigation and elastic behavior of FGM rotary cylinders has been introduced. Assumed cylinder was divided to numerous finite width layers with constant thermodynamic properties in each layer. Governing equations converted to ordinary differential equations with constant coefficients by applying continuity conditions between layers and boundary conditions of disc in derived equations, then these equations could be solved by a prepared computer code. For thermo-elastic part, variation of dimensionless radial and circumferential strains versus dimensionless radius investigated for several power of FGM material. Also, verification of results was done. For creep part, variation of dimensionless radial and circumferential strain rates versus dimensionless radius was studied for different temperatures and limited timeframe. Changes of radial and circumferential strain rates versus radius were investigated and the results were validated. Finally, the effects of various parameters on creep behavior of rotary cylinder in several examples was examined.

Nomenclature

κ, ζ	Material constants for creep	u	Radial displacement
\dot{u}	Radial displacement rate	ν	Poisson ratio
q	Constant of material	ΔT	Temperature gradient in cylinder
L, h	Length and walled thickness of cylinder	n	Power of functional graded material
R_i, R_o	Inner and outer radii of cylinder	ω	Angular velocity of cylinder
Z	A column matrix	$\varepsilon_{rr}, \varepsilon_{\theta\theta}$	Radial and tangential strains
z, θ, r	Components of axial, circumferential and radial directions	P_r	Typical material property
P_o, P_i	Property at the inner and outer surfaces of cylinder	$\dot{\varepsilon}_{rr}, \dot{\varepsilon}_{\theta\theta}$	Strains rate of radial and tangential
$\dot{\sigma}_{rr}, \dot{\sigma}_{\theta\theta}$	Radial and tangential stresses rate	$\dot{\sigma}_{zz}$	Axial stress rate
σ_{eff}	Effective stress	\bar{Z}_1^k, \bar{Z}_2^k	Unknown coefficients of the layer k
τ	Creep time	$\Delta \tau$	Time step
$E_{(r)}, \nu_{(r)}$	Elastic modulus and Poisson ratio in an arbitrary radius	$\dot{\varepsilon}_{rr,c}$	Creep strain rate in radial direction

*Corresponding author: N. Habibi (Associate Professor)
E-mail address: n.habibi@uok.ac.ir

$\dot{\epsilon}_{\theta\theta,c}$	Creep strain rate in tangential direction	$\epsilon_{cr}, \epsilon_{c\theta}$	Creep strain in radial and tangential directions
\bar{E}_i, \bar{E}_o	Inner and outer lateral surfaces dimensionless elasticity modulus	$\bar{E}_{(r)}$	Dimensionless elasticity modulus in an arbitrary radius
ρ_{in}, ρ_{out}	Inner and outer lateral surfaces density of cylinder	$\alpha_{in}, \alpha_{out}$	Inner lateral and outer surfaces thermal expansion coefficient of cylinder
ν_{in}, ν_{out}	Inner and outer lateral surfaces poisson ratio of cylinder	K_{in}, K_{out}	Thermal conductivity coefficient in inner and outer lateral surfaces of cylinder
Al, Cer	Aluminum and Cerami	$\Delta T_i, \Delta T_o$	Temperature gradient in inner and outer lateral surfaces of cylinder

1. Introduction

Recently, by development and growth of powerful engines, turbines, reactors and other machinery, heat and mechanically resistant materials are required. Because of some existing issues in different industries for subjecting materials to high heat stresses, Japanese material scientists in Sundae, for the first time, suggested FG (Functional Graded) materials as high heat resistant materials [1]. FG materials are composite materials with inhomogeneous microstructure that their mechanical properties change from plate to plate in the body smoothly and have certain variations in the material properties. According to composition type, mechanical properties have also continuous variations in thickness direction. Such materials have more effective mechanical properties than layer composite materials, because of continuous composition of former ones. These materials are used in the following applications: In various industries including aerospace (Cape missiles, jet engines), the automotive industry (Hybrid cars), marine industries, construction of advanced turbines.

Generally, to obtain main results, stress in plate, disc, and cylinder should be determined. Sing and Rey [2,3] described steady-state creep analysis of an inhomogeneous rotary cylinder made from composite materials, including silicon carbide particles in special aluminum matrix, by using Hill yielding criterion and Norton law. Material creep parameters of their assumed disc were changing with radius because of proportional variation in composition of silicon carbide particles in the aluminum matrix. Howie shen investigated post-buckling analysis of cylinder panels axially loaded in thermal ambient. This analysis was conducted for FG cylinder panel with finite length [4]. Leo Jacob [5] studied thermoelastic analysis and optimization of plates and FG shells. He used meshless and finite element methods.

Li Yu et al. [6] presented a semi-analytical method for analysis of thermoelastic behavior of hollow cylinders made from targeted materials. They considered constant material properties by dividing cylinder to several cylinders in the radial direction and simplifying equations to solve. Gupta and Singh [7] had studied

anisotropy effect of FG steady-state creep.

In the other study [9] for rotating cylinder, all of the material properties were assumed to be exponentially graded along radius. A semi-analytical solution (the method of successive approximation) was developed to obtain history of stresses and deformations during creep evolution of the EGM rotating cylinder. A comprehensive comparison was made between creep response of homogenous and non-homogenous cylinders. It has been concluded that the material in-homogeneity parameter has a considerable effect on the thermoelastic and creep response of rotating cylinders made of EGMs.

Ghannad et al. [10] investigated an elastic analysis for FGM thick cylindrical shells having axially linear varying thickness utilizing the FSDT. The governing equations in the axisymmetric case and elasto-static state, which are a system of ODE with variable coefficients, were solved analytically using the MAM of the perturbation theory.

Nejad and co-workers [11] investigated time-dependent thermo-elastic creep response for isotropic rotating thick-walled cylindrical pressure vessels made of functionally graded material. Moreover, a semi-analytical method was applied for the purpose of elastic analysis of rotating thick cylindrical shells with variable thicknesses made of axially functional graded material under non-uniform pressure and derived a semi-analytical solution for determination of displacements and stresses in a thick cylindrical shell with variable thicknesses under non-uniform pressure [12-14]. In the study of Jabbari and co-workers [15], the material properties, except the Poisson's ratio, were assumed to vary with the power law function in the axial direction of the pressure vessel. The effects of higher-order approximation on the radial and axial displacements, Von-Mises, and shear stresses were studied. Also, the effects of mechanical and thermal loading, thickness profile type, and gradient index on the mechanical behavior of the cylindrical pressure vessel were examined.

Loghman et al. [16] using Burgers viscoelastic creep model, studied history of strains, stresses, and displacements of a rotating cylinder made of polypropylene reinforced by multi-walled carbon nanotubes (MWCNTs) under magneto-thermo-mechanical loading; it

was discovered that radial displacement, tangential strain, and absolute values of radial strain increase with time at a decreasing rate, finally, approaching the steady-state conditions; effective stresses decreasing at the inner and increase at the outer surface of the cylinder.

Garg and co-workers [17] investigated the steady-state creep in a rotating FGM disc with linearly varying thickness by using von-Mises yield criterion; it was shown that when the FGM disc is subjected to a radial TG (Thermal Gradient), with temperature and radius increasing simultaneously, the radial stress increases over the entire disc but the tangential and effective stresses increase near the inner radius and decrease toward the outer radius. Furthermore, the creep strain rates in rotating FGM disc could be significantly reduced when the disc is subjected to a radial TG, with temperature and radius increasing simultaneously.

In the other research [18] distributions of stress and strain components of rotating discs with non-uniform thickness and material properties subjected to thermo-elastoplastic loading were obtained by semi-exact Liaos homotopy analysis method (HAM) and finite element method (FEM). The materials were assumed to be elastic-linear strain hardening and isotropic. The analysis of rotating disk was based on Von Mises yield criterion. A 2D plane stress analysis was used. The distribution of temperature was assumed to have power forms with the hotter point located at the outer surface of the disk.

Garg et al. [19] studied the steady-state creep behavior of a rotating FGM disc having linearly varying thickness. The disc was assumed to be made of functionally graded composite containing non-linearly varying radial distribution of silicon carbide particles in a matrix of pure aluminum. It was observed that the radial and tangential stresses induced in the FGM disc decrease throughout with the increase in thickness gradient of the disc. The strain rates also decrease with the increase in thickness gradient of the FGM disc, with a relatively higher decrease near the inner radius. The increase in disc thickness gradient results in relatively uniform distribution of strain rates and hence reduces the possibility of distortion in the disc.

Khanna and co-workers studied [20] steady-state creep in a rotating Al-SiCp disc with different thickness profiles and reinforcement (SiCp) gradients. They assumed the disc material to creep according to threshold-stress based law and yield following Tresca criterion. The stress and strain rates in the disc were calculated by using the disc equilibrium equations along with creep constitutive equations. It was observed that on the increase of the disc thickness gradient, the radial stress declines towards the inner radius but increases towards the outer radius, whereas the tangential stress decreases over the entire radius. Also, the composite disc having higher thickness and

higher reinforcement gradients exhibits lesser distortion.

Previous works on this topic have been done more for rotary discs, but in the present research, cylinder made of functional graded materials was investigated that this issue is new in terms of geometry. To solve this problem, the semi-analytical method was used which is different from the method used in other researches.

In this research, analysis of creep behavior of Functional Graded (FG) rotary cylinder was considered (Fig. 1). Derived equations originated from thermo-elasticity theory for FG rotary cylinder by using their displacement equation. According to Norton law (Eq. (1)), also steady-state creep equation of cylinder deduced:

$$\varepsilon_{cr} = \kappa \sigma_{ef}^{\zeta} \tau^q \quad (1)$$

in which κ and ζ are material constants for creep.

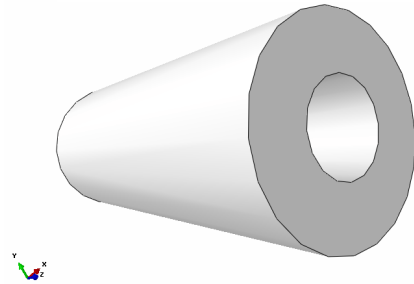


Fig. 1. Schematic view of a cylinder made of FGM material.

In Fig.1 an FGM cylinder with free constraint supported without tangential force, length L , wall thickness h , inner radius R_i and outer radius R_o which rotates with constant angular velocity ω and loaded thermally is considered. In the present research, creep analysis of rotary cylinder made of inhomogeneous materials was conducted. To investigate the effect of important parameters such as gradual change in thermomechanical properties, centrifugal force, thermal loading on stresses, displacements and creep rate of symmetrical rotary inhomogeneous cylinder, an exact method has been suggested. Using this method allows to solve governing equations without any simplification such as considering some properties or coefficients to be constant in radial direction which often considered in creep analysis of inhomogeneous cylinders in mechanic literature. moreover, there is no need to regard derivative of material properties which appeared in equations.

Equilibrium equations based on thermo-elasticity theory for a rotary inhomogeneous cylinder were derived. And then used displacement equation was deduced. To obtain temperature distribution in cylinder, nonlinear heat transfer equation in radial direction was used. Also by using Norton law, equation of steady-state creep for cylinder was derived. To solve derived equations, assumed cylinder was divided into

many layers with finite thicknesses in radial direction and constant thermo-mechanic properties in each layer. By applying continuous conditions between layers and general boundary conditions in obtained equations, a set of algebraic equations would be derived. Cylindrical coordinate system which is placed in the cylinder center layer was used and components z, θ and r are axes, circumferential and thickness directions respectively.

2. Modeling

2.1. Variation of Property in Inhomogeneous Materials

The most common applicant model is volume proportional distribution based on the power law. In this model main assumption is that volume proportion of contributing materials of structure varies just in one direction. For instance, in the body, in thickness direction, mechanical property variation profiles along r is considered as a polynomial of degree n [21].

$$P_r = (P_0 - P_i) \left(\frac{r - R_i}{R_0 - R_i} \right)^n + P_i \quad (2)$$

Dimensionless form of the above equation is [21]:

$$\frac{P_r}{P_i} = \left(\frac{P_0}{P_i} - 1 \right) \left(\frac{r - R_i}{R_0 - R_i} \right)^n + 1 \quad (3)$$

which P_r represents typical material property, P_0 and P_i indicate property at the inner and outer surface of the cylinder respectively. The power n depends on material variation which is variation profile in the thickness direction.

2.2. Governing Thermoelasticity Equations of the FGM Rotary Cylinder Behavior

Consider a cylinder with constant angular velocity ω . It was assumed that this cylinder is under a symmetric

$$\begin{aligned} & \left[\frac{E(r)(1 - \nu(r))}{1 - \nu(r) - 2\nu(r)^2} \right] \frac{d^2 u}{dr^2} + \left[\frac{\nu(r)}{(1 - \nu(r))} \left(\frac{E(r)(1 - \nu(r))}{1 - \nu(r) - 2\nu(r)^2} \right) + \frac{1}{r} \left(\frac{E(r)}{(1 + \nu(r))} \right) + \frac{d}{dr} \left(\frac{E(r)(1 - \nu(r))}{1 - \nu(r) - 2\nu(r)^2} \right) \right] \frac{du}{dr} + \\ & \left[-\frac{\nu(r)}{r^2} \left(\frac{E(r)(1 - \nu(r))}{1 - \nu(r) - 2\nu(r)^2} \right) - \frac{1}{r^2} \left(\frac{E(r)}{1 + \nu(r)} \right) + \left(\frac{\nu(r)}{r} \right) \frac{d}{dr} \left(\frac{E(r)(1 - \nu(r))}{1 - \nu(r) - 2\nu(r)^2} \right) + \frac{1}{r} \frac{d}{dr} \left(\frac{\nu(r)}{(1 - \nu(r))} \right) \left(\frac{E(r)(1 - \nu(r))}{1 - \nu(r) - 2\nu(r)^2} \right) \right] u \\ & + \left[-\left(\frac{E(r)(1 - \nu(r))}{1 - \nu(r) - 2\nu(r)^2} \right) \frac{d}{dr} \left[\left(1 + \frac{\nu(r)}{(1 - \nu(r))} \right) \alpha(r) \Delta T(r) \right] + \rho(r) r \omega^2 - \frac{d}{dr} \left(\frac{E(r)(1 - \nu(r))}{1 - \nu(r) - 2\nu(r)^2} \right) \left(1 + \frac{\nu(r)}{(1 - \nu(r))} \right) \alpha(r) \Delta T(r) \right] = 0 \quad (9) \end{aligned}$$

2.3. The Governing Relations of FGM Rotary Cylinder Creep Behavior

Geometrical relation between strains and rate of radial displacement is:

$$\varepsilon_{rr} = \frac{d\dot{u}}{dr}, \quad \dot{\varepsilon}_{\theta\theta} = \frac{\dot{u}}{r} \quad (10)$$

and variable thermal gradient in radial direction. Volumetric body forces because of centrifugal forces are equal to $\rho r \omega^2$. Since forces were symmetric and functions of radius, shear stress was zero whereas radial and tangential stresses were radius functions. Plane strain will be dominated whenever the cylinder length is long enough, then the problem will be solved by plane stress assumption. The strain-displacement relations in homogeneous rotary cylinder is:

$$\varepsilon_{rr} = \frac{du}{sr}, \quad \varepsilon_{\theta\theta} = \frac{u}{r} \quad (4)$$

In which u is radial displacement, ε_{rr} and $\varepsilon_{\theta\theta}$ are radial and tangential strains respectively. Also stress-strain relations for plane strain conditions are followed by:

$$\sigma_{rr} = \frac{E(r)(1 - \nu(r))}{1 - \nu(r) - 2\nu(r)^2} \times \left[\left(\varepsilon_{rr} + \frac{\nu(r)}{(1 - \nu(r))} \varepsilon_{\theta\theta} \right) - \left(1 + \frac{\nu(r)}{(1 - \nu(r))} \right) \alpha(r) \Delta T(r) \right] \quad (5)$$

$$\sigma_{\theta\theta} = \frac{E(r)(1 - \nu(r))}{1 - \nu(r) - 2\nu(r)^2} \times \left[\left(\varepsilon_{\theta\theta} + \frac{\nu(r)}{(1 - \nu(r))} \varepsilon_{rr} \right) - \left(1 + \frac{\nu(r)}{(1 - \nu(r))} \right) \alpha(r) \Delta T(r) \right] \quad (6)$$

$$\sigma_{zz} = \nu(\sigma_{rr} + \sigma_{\theta\theta}) \quad (7)$$

The equilibrium equation for axial symmetric stress is:

$$\frac{d\sigma_{rr}}{dr} + \frac{\sigma_{rr} - \sigma_{\theta\theta}}{r} + \rho r \omega^2 = 0 \quad (8)$$

In which $\rho r \omega^2$ is volumetric body force because of centrifugal force. By substituting Eq. (4) in Eqs. (5)-(7) and then in Eq. (8) results Navier thermoelastic equation are follows:

According to Norton law, stress-strain rate relationship is:

$$\dot{\sigma}_{rr} = \frac{E(r)(1 - \nu(r))}{1 - \nu(r) - 2\nu(r)^2} \left[\left(\dot{\varepsilon}_{rr} + \frac{\nu(r)}{(1 - \nu(r))} \dot{\varepsilon}_{\theta\theta} \right) - \left(\dot{\varepsilon}_{rr,c} + \frac{\nu(r)}{(1 - \nu(r))} \dot{\varepsilon}_{\theta\theta,c} \right) \right] \quad (11)$$

$$\dot{\sigma}_{\theta\theta} = \frac{E(r)(1-\nu(r))}{1-\nu(r)-2\nu(r)^2} \left[\left(\dot{\varepsilon}_{\theta\theta} + \frac{\nu(r)}{(1-\nu(r))} \dot{\varepsilon}_{rr} \right) - \left(\dot{\varepsilon}_{\theta\theta,c} + \frac{\nu(r)}{(1-\nu(r))} \dot{\varepsilon}_{rr,c} \right) \right] \quad (12)$$

And

$$\sigma_{eff} = \sqrt{\sigma_{rr}^2 - (\sigma_{rr} \times \sigma_{\theta\theta}) + \sigma_{\theta\theta}^2} \quad (16)$$

$$\dot{\sigma} = \nu(\dot{\sigma}_{rr}, \dot{\sigma}_{\theta\theta}) \quad (13)$$

By using Eq. (8), equilibrium equation for stress rates will be:

In which:

$$\dot{\varepsilon}_{rr,c} = \frac{\kappa\sigma_{eff}^{\zeta-1}}{2q} (2\sigma_{rr} - \sigma_{\theta\theta}) \left(\frac{\varepsilon_{cr}}{\kappa\sigma_{eff}^{\zeta}} \right)^{\frac{q-1}{q}} \quad (14) \quad \frac{d\dot{\sigma}_{rr}}{dr} + \frac{\dot{\sigma}_{rr} - \dot{\sigma}_{\theta\theta}}{r} = 0 \quad (17)$$

$$\dot{\varepsilon}_{\theta\theta,c} = \frac{\kappa\sigma_{eff}^{\zeta-1}}{2q} (2\sigma_{\theta\theta} - \sigma_{rr}) \left(\frac{\varepsilon_{cr}}{\kappa\sigma_{eff}^{\zeta}} \right)^{\frac{q-1}{q}} \quad (15)$$

Substituting Eq. (10) in Eq. (11) and Eq. (12) and then in Eq. (17) results governing equation of FGM rotary cylinder creep behavior are followed by:

$$\begin{aligned} & \left[\frac{E(r)(2-\nu(r))}{1-\nu(r)-2\nu(r)^2} \right] \frac{d^2 \dot{u}}{dr^2} + \left[\frac{\nu(r)}{(1-\nu(r))r} \left(\frac{E(r)(1-\nu(r))}{1-\nu(r)-2\nu(r)^2} \right) + \frac{1}{r} \left(\frac{E(r)}{1+\nu(r)} \right) + \frac{d}{dr} \left(\frac{E(r)(1-\nu(r))}{1-\nu(r)-2\nu(r)^2} \right) \right] \frac{d\dot{u}}{dr} \\ & + \left[-\frac{\nu(r)}{(1-\nu(r))r} \left(\frac{E(r)(1-\nu(r))}{1-\nu(r)-2\nu(r)^2} \right) - \frac{1}{r^2} \left(\frac{E(r)}{1+\nu(r)} \right) + \left(\frac{\nu(r)}{(1-\nu(r))r} \right) \frac{d}{dr} \left(\frac{E(r)(1-\nu(r))}{1-\nu(r)-2\nu(r)^2} \right) + \frac{1}{r} \frac{d}{dr} \left(\frac{\nu(r)}{(1-\nu(r))} \left(\frac{E(r)(1-\nu(r))}{1-\nu(r)-2\nu(r)^2} \right) \right) \right] \dot{u} \\ & + \left[-\left(\frac{E(r)(1-\nu(r))}{1-\nu(r)-2\nu(r)^2} \right) \frac{d}{dr} \left(\frac{\nu(r)}{(1-\nu(r))} \right) - \left(\frac{E(r)}{1+\nu(r)} \right) \frac{1}{r} - \frac{d}{dr} \left(\frac{E(r)(1-\nu(r))}{1-\nu(r)-2\nu(r)^2} \right) \right] \dot{\varepsilon}_{\theta,c} \\ & + \left[\left(\frac{E(r)}{1+\nu(r)} \right) \frac{1}{r} - \frac{\nu(r)}{(1-\nu(r))} \frac{d}{dr} \left(\frac{E(r)(1-\nu(r))}{1-\nu(r)-2\nu(r)^2} \right) \right] \dot{\varepsilon}_{\theta,c} \\ & + \left[-\frac{\nu(r)}{(1-\nu(r))} \left(\frac{E(r)(1-\nu(r))}{1-\nu(r)-2\nu(r)^2} \right) \right] \frac{d\dot{\varepsilon}_{\theta,c}}{dr} + \left[-\left(\frac{E(r)(1-\nu(r))}{1-\nu(r)-2\nu(r)^2} \right) \right] \frac{d\dot{\varepsilon}_{\theta,c}}{dr} = 0 \quad (18) \end{aligned}$$

2.4. Boundary Conditions

The boundary condition problems will be reviewed in three different cases then introduced briefly in the following.

2.4.1. Hollow Cylinder with Free Edges

It was assumed that inner and outer cylinder surfaces are free and without any constraint; also they are not subjected to external forces. Hence these boundary conditions are applied to the cylinder as follows:

$$\begin{aligned} \sigma_{rr} &= 0 \quad \text{at} \quad t = R_i \\ \sigma_{rr} &= 0 \quad \text{at} \quad t = R_o \end{aligned} \quad (19)$$

2.4.2. Hollow Cylinder with Fixed-Free Edges

It was assumed that the cylinder has no radial displacement in the inner surface but the outer surface is free

and there is no movement constraint.

$$\begin{aligned} u &= 0 \quad \text{at} \quad r = R_i \\ \sigma_{rr} &= 0 \quad \text{at} \quad t = R_o \end{aligned} \quad (20)$$

2.4.3. Filled Cylinder with Free Edges

It was assumed that the cylinder has no radial displacement in its centerline (cylinder is assumed filled) but the outer surface is free and there is no movement constraint.

$$\begin{aligned} u &= 0 \quad \text{at} \quad r = 0 \\ \sigma_{rr} &= 0 \quad \text{at} \quad r = R_o \end{aligned} \quad (21)$$

2.5. The Solving Algorithm

Direct solving of Eq. (9) and Eq. (18) is impossible because all of the parameters are functions of rotary cylinder radius, r . Hence some simplifying or special solving methods are required to solve the equations. In this research, a semi-analytical method to solve recent equations has been introduced. Here the solving method

for governing equations of FGM rotary cylinder creep (Eq. (18)) is introduced and for solving Navier thermoelastic, Eq. (9), a similar method is applied. In this method, the studying cylinder is divided into many layers with t^k thickness that superscript k , indicates layer k . By considering constant material properties in each layer and replacing r^k rather than r which r^k indicates

mean radius of layer k , In the desired relation, Eq. (18) converts to ordinary differential equation with constant coefficients as follows:

$$\left(\bar{c}_1^k \frac{d^2}{dr^2} + \bar{c}_2^k \frac{d}{dr} + \bar{c}_3^k\right) \dot{u}^k + \bar{c}_1^k = 0 \quad (22)$$

In which:

$$\bar{c}_1^k = \frac{E(r)(1 - \nu(r))}{1 - \nu(r) - 2\nu(r)^2} \quad (23a)$$

$$\bar{c}_2^k = \frac{\nu(r)}{r^k} \left(\frac{E(r)(1 - \nu(r))}{1 - \nu(r) - 2\nu(r)^2} \right) + \frac{1}{r^k} \left(\frac{E(r)(1 - \nu(r))}{1 - \nu(r) - 2\nu(r)^2} \right) + \frac{d}{dr} \left(\frac{E(r)(1 - \nu(r))}{1 - \nu(r) - 2\nu(r)^2} \right) \Big|_{r=r^k} \quad (23b)$$

$$\begin{aligned} \bar{c}_3^k &= \frac{\nu(r)}{r^k} \left(\frac{E(r)(1 - \nu(r))}{1 - \nu(r) - 2\nu(r)^2} \right) \frac{1}{h_{(r^k)}} \frac{dh_{(r)}}{dr} \Big|_{r=r^k} - \frac{\nu(r)}{r^{k^2}} \left(\frac{E(r)(1 - \nu(r))}{1 - \nu(r) - 2\nu(r)^2} \right) - \frac{1}{r^{k^2}} \left(\frac{E(r^k)}{1 + \nu(r^k)} \right) \\ &+ \left(\frac{\nu(r)}{(1 - \nu(r))} \right) \frac{d}{dr} \left(\frac{E(r)(1 - \nu(r))}{1 - \nu(r) - 2\nu(r)^2} \right) \Big|_{r=r^k} + \frac{1}{r^k} \left(\frac{E(r)(1 - \nu(r))}{1 - \nu(r) - 2\nu(r)^2} \right) \frac{d}{dr} \left(\frac{\nu(r)}{(1 - \nu(r))} \right) \Big|_{r=r^k} \end{aligned} \quad (23c)$$

$$\begin{aligned} \bar{c}_4^k &= \left[- \left(\frac{E(r)(1 - \nu(r))}{1 - \nu(r) - 2\nu(r)^2} \right) \frac{d}{dr} \left(\frac{\nu(r)}{(1 - \nu(r))} \right) \Big|_{r=r^k} - \frac{1}{r^k} \left(\frac{E(r^k)}{1 + \nu(r^k)} \right) - \frac{d}{dr} \left(\frac{E(r)(1 - \nu(r))}{1 - \nu(r) - 2\nu(r)^2} \right) \Big|_{r=r^k} \right] \dot{\varepsilon}_{rr,c} \\ &+ \left[\frac{1}{r^k} \left(\frac{E(r^k)}{1 + \nu(r^k)} \right) - \frac{\nu(r)}{(1 - \nu(r))} \times \frac{d}{dr} \left(\frac{E(r)(1 - \nu(r))}{1 - \nu(r) - 2\nu(r)^2} \right) \Big|_{r=r^k} \right] \dot{\varepsilon}_{\theta,\theta,c} \\ &+ \left[- \frac{\nu(r)}{(1 - \nu(r))} \left(\frac{E(r)(1 - \nu(r))}{1 - \nu(r) - 2\nu(r)^2} \right) \right] \frac{d\dot{\varepsilon}_{rr,c}}{dr} + \left[- \left(\frac{E(r)(1 - \nu(r))}{1 - \nu(r) - 2\nu(r)^2} \right) \right] \frac{d\dot{\varepsilon}_{\theta,\theta,c}}{dr} \end{aligned} \quad (23d)$$

To calculate value of $\frac{d\dot{\varepsilon}_{rr,c}}{dr}$ and $\frac{d\dot{\varepsilon}_{\theta,\theta,c}}{dr}$ following relations are used:

$$\left(\frac{d\dot{\varepsilon}_{rr,c}}{dr} \right) = (\dot{\varepsilon}_{rr,c}^{k+1} - \dot{\varepsilon}_{rr,c}^k) / (r^{k+1} - r^k) \quad (24)$$

$$\left(\frac{d\dot{\varepsilon}_{\theta,\theta,c}}{dr} \right)^{k+1} = (\dot{\varepsilon}_{\theta,\theta,c}^{k+1} - \dot{\varepsilon}_{\theta,\theta,c}^k) / (r^{k+1} - r^k) \quad (25)$$

The Eq. (22) can be written for any layer distinctly. So if the cylinder has m layers, there are m ordinary differential equations with constant coefficients. The advantage of using this method is that an exact solution of Eq. (22) exists as:

$$\dot{u}_{(r)}^k = \bar{z}_1^k \exp(\lambda_1^k r) + \bar{z}_2^k \exp(\lambda_2^k r) - \frac{\bar{c}_4^k}{\bar{c}_3^k} \quad (26)$$

$$r^k - \frac{t^k}{2} < r < r^k + \frac{t^k}{2}$$

In which:

$$\lambda_1^k, \lambda_2^k = - \left(\frac{\bar{c}_2^k \pm \sqrt{\bar{c}_3^k - 4\bar{c}_1^k \bar{c}_3^k}}{2\bar{c}_1^k} \right) \quad (27)$$

The coefficients specified as \bar{Z}_1^k and \bar{Z}_2^k are unknown coefficients of the layer k in the equation. By applying

boundary conditions between any two adjacent layers which are the same for stress and displacement rate continuity in the radial direction of that layers as well:

$$\dot{u}_{(r^k + \frac{t^k}{2})}^k = \dot{u}_{(r^{k+1} - \frac{t^{k+1}}{2})}^{k+1} \quad (28)$$

$$\dot{\sigma}_{rr}^k \Big|_{r=r^k + \frac{t^k}{2}} = \dot{\sigma}_{rr}^{k+1} \Big|_{r=r^{k+1} - \frac{t^{k+1}}{2}} \quad (29)$$

A set of m equations will be obtained from applying boundary conditions in Eq. (26) with continuity, Eq. (28) and Eq. (29) are represented as follows:

$$[F]_{m \times m} [Z]_{m \times 1} = [G]_{m \times 1} \quad (30)$$

in which matrix Z is a column matrix that its arrays are unknown values of the equation. Square matrix F and column matrix G will derive from continuity condition among layers as well as the whole cylinder. There is a solution method for the cylinder with boundary conditions in Eq. (31) and the same manner for other boundary conditions is applied.

$$\dot{\sigma}_{rr} = 0 \quad \text{at} \quad t = R_i \quad (31)$$

$$\dot{\sigma}_{rr} = 0 \quad \text{at} \quad t = R_o$$

By substituting the cylinder inner surface boundary conditions in Eq. (26), the equation of radial displacement rate will be:

$$\dot{u}_{(R_i)}^1 = \bar{Z}_1^1 \exp(\lambda_1 r) + \bar{Z}_2^1 \exp(\lambda_2 r) - \frac{\bar{c}_4^1}{\bar{c}_3^1} \quad (32)$$

By putting $\dot{u}_{(R_i)}^1$ taken from above in Eq. (10) and then in Eq. (11), radial stress rate in the surface of cylinder will be obtained zero according to the boundary conditions:

$$\begin{aligned} & \frac{E_i(1-\nu_i)}{1-\nu_i-2\nu_i^2} \left[\bar{Z}_1^1 \lambda_1^1 \exp(\lambda_1^1 R_i) + \bar{Z}_2^1 \lambda_2^1 \exp(\lambda_2^1 R_i) + \right. \\ & \left. \left(\left(\frac{\nu_i}{(1-\nu_i)} \right) / R_i \right) \left(\bar{Z}_1^1 \lambda_1^1 \exp(\lambda_1^1 R_i) + \bar{Z}_2^1 \lambda_2^1 \exp(\lambda_2^1 R_i) - \frac{\bar{c}_4^1}{\bar{c}_3^1} \right) \right. \\ & \left. - \left(\dot{\epsilon}_{rr,c}^1 + \frac{\nu_i}{(1-\nu_i)} \dot{\epsilon}_{\theta\theta,c}^1 \right) \right] = 0 \quad (33) \end{aligned}$$

So the values of F_{11} and F_{12} and G_1 are:

$$\begin{aligned} F_{11} &= \frac{E_i(1-\nu_i)}{1-\nu_i-2\nu_i^2} \left[\lambda_1^1 \exp(\lambda_1^1 R_i) + \left(\frac{\nu_i}{R_i(1-\nu_i)} \right) \exp(\lambda_1^1 R_i) \right] \\ F_{12} &= \frac{E_i(1-\nu_i)}{1-\nu_i-2\nu_i^2} \left[\lambda_2^1 \exp(\lambda_2^1 R_i) + \left(\frac{\nu_i}{R_i(1-\nu_i)} \right) \exp(\lambda_2^1 R_i) \right] \\ G_1 &= \frac{E_i(1-\nu_i)}{1-\nu_i-2\nu_i^2} \left[\left(\frac{\nu_i}{(1-\nu_i)} \right) - \frac{\bar{c}_4^1}{\bar{c}_3^1} + \left(\dot{\epsilon}_{rr,c}^1 + \frac{\nu_i}{(1-\nu_i)} \dot{\epsilon}_{\theta\theta,c}^1 \right) \right] \quad (34) \end{aligned}$$

The radial stress relation in the cylinder outer surface will be obtained in the same manner by using the above values $F_{(2m)(2m-1)}$, $F_{(2m)(2m)}$, and $G_{(2m)}$, represented

as follows:

$$F_{(2m)(2m-1)} = \frac{E_o(1-\nu_o)}{1-\nu_o-2\nu_o^2} \left[\lambda_1^m \exp(\lambda_1^m R_o) + \frac{\nu_o}{R_o} \exp(\lambda_1^m R_o) \right]$$

$$F_{(2m)(2m)} = \frac{E_o(1-\nu_o)}{1-\nu_o-2\nu_o^2} \left[\lambda_2^m \exp(\lambda_2^m R_o) + \frac{\nu_o}{R_o} \exp(\lambda_2^m R_o) \right]$$

$$G_{(2m)} = \frac{E_o(1-\nu_o)}{1-\nu_o-2\nu_o^2} \left[\left(\frac{\nu_o}{R_o(1-\nu_o)} \right) \frac{\bar{c}_4^m}{\bar{c}_3^m} + \left(\dot{\epsilon}_{rr,c}^m + \left(\frac{\nu_o}{(1-\nu_o)} \right) \dot{\epsilon}_{\theta\theta,c}^m \right) \right] \quad (35)$$

By putting Eq. (26) in continuity condition of radial displacement rate (Eq. (28)), values of the $F_{(2k)(2k-1)}$, $F_{(2k)(2k)}$ and $G_{(2k)}$ are:

$$F_{(2k)(2k-1)} = \exp \left(\lambda_1^k \left(r^k + \frac{t^k}{2} \right) \right)$$

$$F_{(2k)(2k)} = \exp \left(\lambda_2^k \left(r^k + \frac{t^k}{2} \right) \right)$$

$$F_{(2k)(2k+1)} = -\exp \left(\lambda_1^{k+1} \left(r^{k+1} + \frac{t^{k+1}}{2} \right) \right) \quad (36)$$

$$F_{(2k)(2k+2)} = -\exp \left(\lambda_2^{k+1} \left(r^{k+1} + \frac{t^{k+1}}{2} \right) \right)$$

$$G_{(2k)} = \frac{\bar{c}_4^m}{\bar{c}_3^m} - \frac{\bar{c}_4^{k+1}}{\bar{c}_3^{k+1}}$$

Also by putting Eq. (26) in continuity condition of radial stress rate, Eq. (28), the values of arrays $F_{(2k+1)(2k-1)}$, $F_{(2k+1)(2k)}$, $F_{(2k+1)(2k+1)}$, $F_{(2k+1)(2k+2)}$ and $G_{(2k+1)}$ are:

$$F_{(2k+1)(2k-1)} = \frac{E_{(r^k)}(1-\nu_{(r^k)})}{1-\nu_{(r^k)}-2\nu_{(r^k)}^2} \left[\lambda_1^k \exp \left(\lambda_1^k \left(r^k + \frac{t^k}{2} \right) \right) + \left(\left(\frac{\nu_{(r^k)}}{(1-\nu_{(r^k)})} \right) / \left(r^k + \frac{t^k}{2} \right) \right) \exp \left(\lambda_1^k \left(r^k + \frac{t^k}{2} \right) \right) \right] \quad (37a)$$

$$F_{(2k+1)(2k)} = \frac{E_{(r^k)}(1-\nu_{(r^k)})}{1-\nu_{(r^k)}-2\nu_{(r^k)}^2} \left[\lambda_2^k \exp \left(\lambda_2^k \left(r^k + \frac{t^k}{2} \right) \right) + \left(\left(\frac{\nu_{(r^k)}}{(1-\nu_{(r^k)})} \right) / \left(r^k + \frac{t^k}{2} \right) \right) \exp \left(\lambda_2^k \left(r^k + \frac{t^k}{2} \right) \right) \right] \quad (37b)$$

$$\begin{aligned} F_{(2k+1)(2k+1)} &= \frac{E_{(r^{k+1})}(1-\nu_{(r^{k+1})})}{1-\nu_{(r^{k+1})}-2\nu_{(r^{k+1})}^2} \left[\lambda_1^{k+1} \exp \left(\lambda_1^{k+1} \left(r^{k+1} - \frac{t^{k+1}}{2} \right) \right) \right. \\ & \left. + \left(\left(\frac{\nu_{(r^{k+1})}}{(1-\nu_{(r^{k+1})})} \right) / \left(r^{k+1} - \frac{t^{k+1}}{2} \right) \right) \exp \left(\lambda_1^{k+1} \left(r^{k+1} - \frac{t^{k+1}}{2} \right) \right) \right] \quad (37c) \end{aligned}$$

$$\begin{aligned} F_{(2k+1)(2k+2)} &= \frac{E_{(r^{k+1})}(1-\nu_{(r^{k+1})})}{1-\nu_{(r^{k+1})}-2\nu_{(r^{k+1})}^2} \left[\lambda_2^{k+1} \exp \left(\lambda_2^{k+1} \left(r^{k+1} - \frac{t^{k+1}}{2} \right) \right) \right. \\ & \left. + \left(\left(\frac{\nu_{(r^{k+1})}}{(1-\nu_{(r^{k+1})})} \right) / \left(r^{k+1} - \frac{t^{k+1}}{2} \right) \right) \exp \left(\lambda_2^{k+1} \left(r^{k+1} - \frac{t^{k+1}}{2} \right) \right) \right] \quad (37d) \end{aligned}$$

$$G_{2k+1} = \frac{E_{(r^k)}(1 - \nu_{(r^k)})}{1 - \nu_{(r^k)} - 2\nu_{(r^k)}^2} \left[\left(\left(\frac{\nu_{(r^k)}}{1 - \nu_{(r^k)}} \right) / \left(r^k + \frac{t^k}{2} \right) \right) \left(\frac{\bar{c}_4^k}{\bar{c}_3^k} \right) + \left(\dot{\varepsilon}_{rr,c}^k + \left(\frac{\nu_{(r^k)}}{1 - \nu_{(r^k)}} \right) \dot{\varepsilon}_{\theta\theta,c}^k \right) \right] \\ - \frac{E_{(r^{k+1})}(1 - \nu_{(r^{k+1})})}{1 - \nu_{(r^{k+1})} - 2\nu_{(r^{k+1})}^2} \left[\left(\left(\frac{\nu_{(r^{k+1})}}{1 - \nu_{(r^{k+1})}} \right) / \left(r^{k+1} - \frac{t^{k+1}}{2} \right) \right) \frac{\bar{c}_4^{-k+1}}{\bar{c}_3^{-k+1}} + \left(\dot{\varepsilon}_{rr,c}^{k+1} + \left(\frac{\nu_{(r^{k+1})}}{1 - \nu_{(r^{k+1})}} \right) \dot{\varepsilon}_{\theta\theta,c}^{k+2} \right) \right] \quad (37e)$$

So the values of matrixes F and G are specified. In order to obtain unknown coefficient (matrix Z), it is required to multiply inverse of matrix F in matrix G . It means that:

$$[Z] = [F]^{-1}[G] \quad (38)$$

So the values of \bar{Z}_2, \bar{Z}_1 are specified for each layer. By substituting \bar{Z}_1^k, \bar{Z}_2^k in Eq. (26), radial displacement rate is determined in any disc point. By specifying radial displacement rate, the stress rates, also, radial and tangential strain rates, can be determined in any cylinder point. Notice that in this study the nonlinear heat transfer equation in radial direction of FGM rotary cylinder was extracted to calculate the cylinder temperature distribution; in order to solve it, a similar method was employed which was presented before in Eq. (18). An appropriate algorithm solution is required to solve the creep governing equation of FGM rotary cylinder which is described in the following. According to this algorithm, solution steps for creep analysis of rotary cylinder made of FG material are:

Step 1: Calculate temperature distribution of the whole disc.

Step 2: Calculate disc displacement and stress-strain distributions.

Step 3: Calculate radial and tangential strain rate distributions using transient creep coefficients.

Step 4: Calculate radial displacement rate distributions and stress rate distribution.

Step 5: Select appropriate time step ($\Delta\tau$) and then calculate new stresses and strains in radial and tangential directions:

$$\begin{aligned} (\sigma_{rr})_{New} &= (\dot{\sigma}_{rr})_{old}\Delta\tau + (\sigma_{rr})_{old} \\ (\sigma_{\theta\theta})_{New} &= (\dot{\sigma}_{\theta\theta})_{old}\Delta\tau + (\sigma_{\theta\theta})_{old} \\ (\varepsilon_{rr})_{New} &= (\dot{\varepsilon})_{old}\Delta\tau + (\varepsilon_{rr})_{old} \\ (\varepsilon_{\theta\theta})_{New} &= (\dot{\varepsilon}_{\theta\theta})_{old}\Delta\tau + (\varepsilon_{\theta\theta})_{old} \end{aligned} \quad (39)$$

Step 6: Repeat steps 4 through 8 until radial and tangential stress distribution rates converge to an invariant value.

Step 7: Calculate radial and tangential strains rate distribution using transient creep coefficients.

Step 8: Calculate radial displacement and stress rates distribution.

3. Results and Discussion

In this section, results of creep analysis of the FGM cylinder from the study was extracted and verified with results from references. In the following, parametric study of structure was conducted, in order to investigate geometrical and mechanical specification effects on the cylinder behavior.

3.1. Verification

In this part, the results of the FGM cylinder creep analysis are compared with the results derived from appropriate references.

3.1.1. First Example

In this example, the study results are compared to creep analysis results of the FGM rotary cylinder provided by Sing and Rey [2]. The disc boundary conditions are:

$$\begin{aligned} R_i &= 31.75mm, & R_o &= 152.4mm \\ \Delta T_i &= \Delta T_o = 561^{\circ}k, \\ w &= 15000rpm \end{aligned}$$

This comparison was made for radial and tangential displacement rates which is shown in Figs. 2 and 3. As shown, a good agreement is established between the research results and the mentioned article.

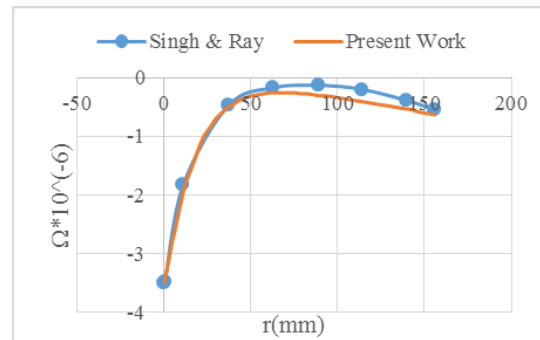


Fig. 2. Comparison between radial displacement rate distribution results and the results in [2]. $\Omega = \dot{\varepsilon}_r (s^{-1})$

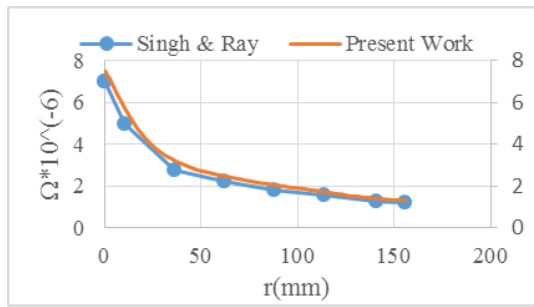


Fig. 3. Comparison between tangential displacement rate distribution results and the results in [2]. $\Omega = \dot{\epsilon}_\theta (s^{-1})$

In Figs. 2 and 3, in special case, by considering plain strain assumption and taking a thin layer of creep investigated., the results of the research and ref.2 are consistent. In general, model (rotating cylinder) and method (semi-analytical) used in the present study are different to the existing references. Also, the rotating cylinder creep is investigated in this paper, while in the ref. 2 creep for thin disc has been investigated.

3.1.2. Second Example

A rotary disc with dimensionless elasticity modulus is considered as below:

$$\bar{E}_{(r)} = \bar{E}_i + (\bar{E}_o - \bar{E}_i) \left(\frac{r - R_i}{R_o - R_i} \right)^n \quad (40)$$

In which \bar{E}_i, \bar{E}_o are dimensionless elasticity modulus of the inner and outer disc layer ingredients respectively. J.F. Durodola and co-workers [8] used two methods, the direct integrating method and the finite element method, to solve the governing equations. To compare results, $\bar{E}_i = \frac{2}{3}, \bar{E}_o = 1, n = 1, R_o = 5R_i$ and double-edge disc boundary conditions were considered. To verify provided results, the dimensionless displacement and stress distribution curves in radial direction, shown in Figs. 4 and 5, were used.

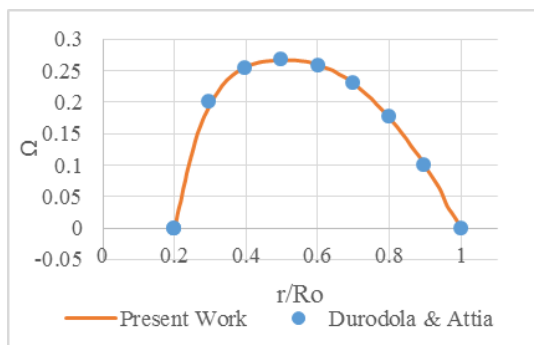


Fig. 4. Comparison between radial stress distribution and finite element method results. $\Omega = \sigma_r / \rho_m w^2 R_o^2$

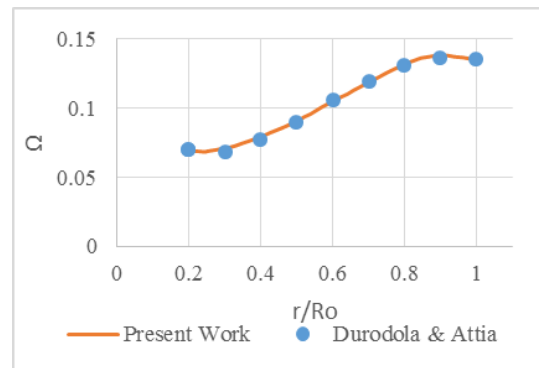


Fig. 5. Comparison between radial displacement distribution and finite element method results.

$$\Omega = u_r E_m / \rho_m w^2 R_o^2$$

As it can be seen, a good agreement exists between the research results and the result induced from the finite element method in the mentioned article.

3.1.3. Parametric Study and Creep Analysis Results Presentations of a Symmetric Loaded FGM Cylinder

In this section, effects of various parameters on creep analysis of FGM cylinder are investigated. In the two following examples, the effects of power of FG properties variation function, n , and thermal gradient magnitude on creep behavior of the FGM rotary cylinder are studied. In the examples, aluminum and zirconium were used as metal and ceramic on the inner and outer cylinder surfaces respectively with their specifications listed as below:

$$\alpha_{in} = \alpha_{Al} = 2.3 \times 10^{-5} / K,$$

$$\alpha_{out} = \alpha_{Cer} = 1 \times 10^{-5} \frac{1}{0 K}$$

$$E_{in} = E_{Al} = 70 Gpa,$$

$$E_{out} = E_{Cer} = 151 Gpa$$

$$\nu_{in} = \nu_{Al} = 0.33,$$

$$\nu_{out} = \nu_{Cer} = 0.31$$

$$K_{in} = K_{Al} = 209 \frac{j}{kg \cdot 0 K},$$

$$K_{out} = K_{Cer} = 2 \frac{j}{kg \cdot 0 K}$$

$$\rho_{in} = \rho_{Al} = 2700 \frac{kg}{m^3},$$

$$\rho_{out} = \rho_{Cer} = 5700 \frac{kg}{m^3}$$

$$\kappa = 9.9 \times 10^{-56}, \zeta = 5.4, q = 0.5$$

Also boundary conditions were considered as Eq. (19) and Eq. (31). To maintain generality and accuracy of examination, the results were normalized. For this reason, radial and tangential strains and also their rates were normalized by means of $\rho_{Cer} w^2 R_o^2 / E_{Cer}$.

3.1.4. Evaluation of the Creep Results of FGM Cylinder in Different Powers

In this case, the values of 0.2, 0.5, 1.5 and 2 were considered as the power of ingredient variation function, n , then its influence was studied on the steady-state creep

behavior of FG rotary cylinder. The specifications of desired cylinder are given below:

$$R_i = 10cm, \quad R_o = 25cm, \quad \Delta T_i = 500^0C$$

$$\Delta T_o = 700^0C, \quad w = 150000rpm$$

Figs. 6 and 7 show radial and tangential normalized strain distribution curves in radial direction of the cylinder equal to 10.88 hours after the start of creep for different power, n , also pure metal/ceramic base are shown too. In both figures by increasing n , the variation range of related strains in the radial direction increases that can be explained by increasing n ; the cylinder properties approach to the properties of a pure metal base cylinder, which has a smaller modulus of elasticity.

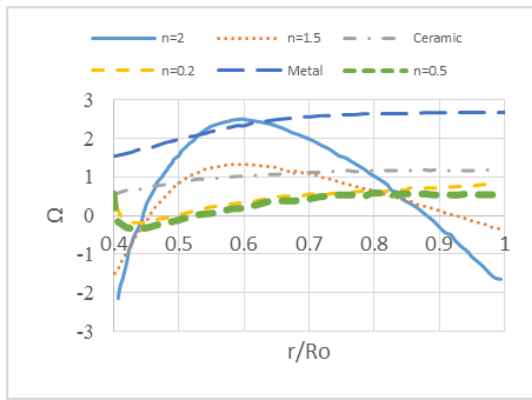


Fig. 6. Dimensionless radial strain distributions in radius direction of cylinder for different powers n . $\Omega = \epsilon_r E_{Cer} / \rho_{Cer} w^2 R_o^2$

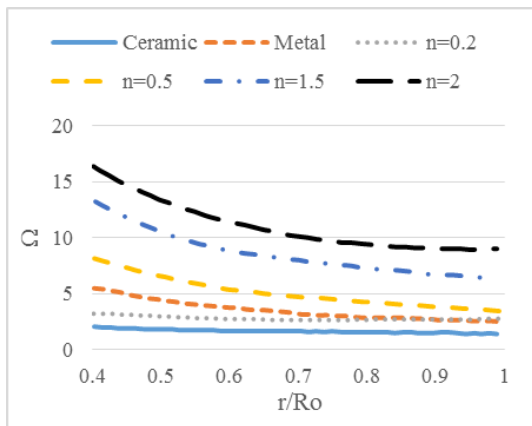


Fig. 7. Dimensionless tangential strain distributions in radius direction of cylinder for different powers n . $\Omega = \epsilon_\theta E_{Cer} / \rho_{Cer} w^2 R_o^2$

According to Fig. 6, in areas close to the inner and outer cylinder surfaces, the radial strain approaches zero with positive values then to negative values by growing n , however in the middle areas of the cylinder the amount of radial strains increase in positive

direction by increasing n . It is obvious in Fig. 7 that tangential strains increase by n in positive direction in the whole cylinder.

3.1.5. Study of Temperature Effect on the FGM Rotary Cylinder Creep

For the investigation of temperature effect on the FGM rotary cylinder creep, a cylinder with the following specifications was considered which was subjected to different temperature gradients.

$$R_i = 10cm, \quad R_o = 30cm, \quad n = 1.5, \quad w = 12000rpm$$

In Figs. 8-11 dimensionless radial and tangential strain distributions are shown in radius direction of cylinder after 10.88 hours from creep start for five different thermal gradients. Fig. 8 shows that increasing in temperature gradient causes rise of radial strain in areas near the inner surface of the cylinder, in negative direction, in the middle, and in positive direction, but descending radial strain in areas near the outer surface of the cylinder.

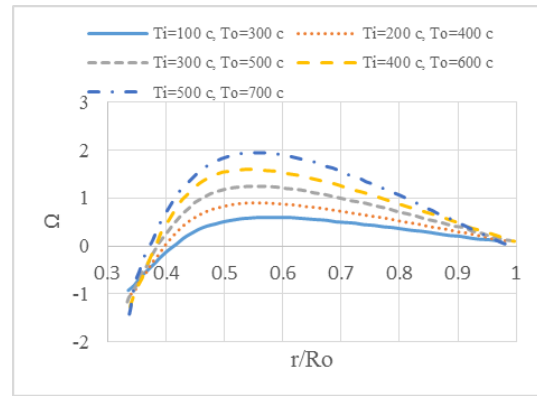


Fig. 8. Dimensionless radial strain distributions in radius direction of cylinder for different gradients. $\Omega = \epsilon_r E_{Cer} / \rho_{Cer} w^2 R_o^2$

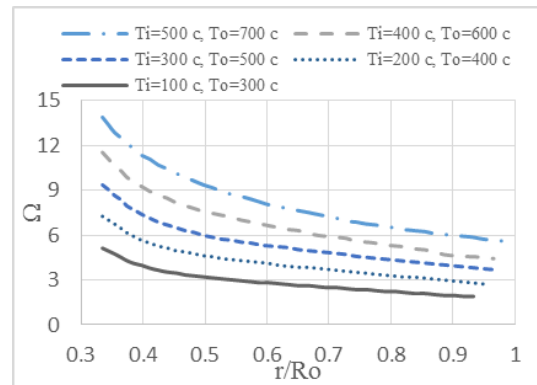


Fig. 9. Dimensionless tangential strain distributions in radius direction of cylinder for different gradients. $\Omega = \epsilon_\theta E_{Cer} / \rho_{Cer} w^2 R_o^2$

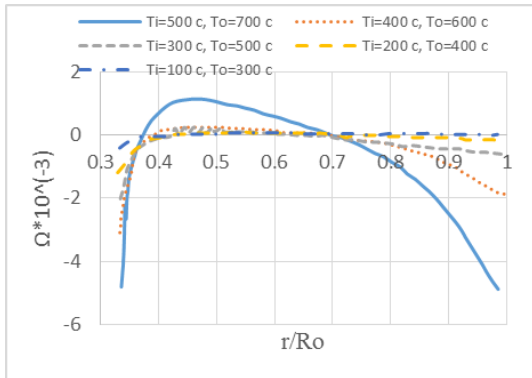


Fig. 10. Dimensionless radial strain rate distributions in radius direction of cylinder for different gradients. $\Omega = \dot{\epsilon}_r E_{Cer} / \rho_{Cer} w^2 R_o^2$

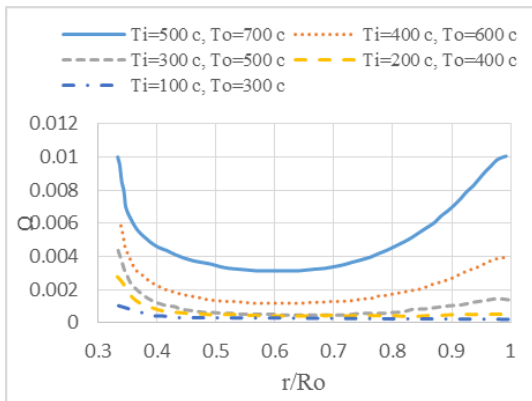


Fig. 11. Dimensionless tangential strain rate distribution in radius direction of cylinder for different gradients. $\Omega = \dot{\epsilon}_\theta E_{Cer} / \rho_{Cer} w^2 R_o^2$

According to Fig.9, it is observed that increase in thermal gradient causes tangential strain rise in the whole cylinder. Fig.10 shows that the absolute values of radial strain rates will increase by thermal gradient. Notice this growth of radial strain rate is not related to linear thermal gradient increment. Also by increasing thermal gradient, amount of tangential strain rate will grow in the whole cylinder, in positive direction (Fig. 11).

3.1.6. Study of Creep Stress and Strain Rates on the FGM Cylinder

In this case, aluminum and zirconium used as metal and ceramic for the inner and outer surfaces of the cylinder respectively. The material properties applied in numerical calculations are as follows:

$$\alpha_{in} = \alpha_{Al} = 2.3 \times 10^{-5} \frac{1}{K},$$

$$\alpha_{out} = \alpha_{Cer} = 1 \times 10^{-5} \frac{1}{K}$$

$$E_{in} = E_{Al} = 70Gpa, \quad E_{out} = E_{Cer} = 151Gpa$$

$$\nu_{in} = \nu_{Al} = 0.33, \quad \nu_{out} = \nu_{Cer} = 0.31$$

$$K_{in} = K_{Al} = 209 \frac{j}{kg \cdot ^0 K}, \quad K_{out} = K_{Cer} = 2 \frac{j}{kg \cdot ^0 K}$$

$$\rho_{in} = \rho_{Al} = 2700 \frac{kg}{m^3}, \quad \rho_{out} = \rho_{Cer} = 5700 \frac{kg}{m^3}$$

$$\kappa = 9.9 \times 10^{-56}, \quad \zeta = 5.4, \quad q = 0.5$$

The boundary conditions are:

$$u_{rr} \quad \text{at} \quad r = R_i \quad \dot{u}_{rr} = 0 \quad \text{at} \quad r = R_i$$

$$\sigma_{rr} = 0 \quad \text{at} \quad r = R_o \quad \dot{\sigma}_{rr} = 0 \quad \text{at} \quad r = R_o$$

The inner radius is 20cm and the outer radius is 50cm which their corresponding surface temperatures at 100 and 300 degrees on the Celsius scale respectively, and it rotates with a 3000 rpm angular velocity. It is assumed that all parameters change will vary in radial direction based on the power law distribution model, using volumetric proportion with variation power 1.5. Figs. 14 and 15 show radial and tangential stress and strain rate distribution curves versus time in three, inner, middle and outer layers. As it can be seen, the outer and inner layers have maximum and minimum stress rates (for both stress rates), for all time respectively. Also, stress rate approaches zero by increasing creep time which occurs from large quantities to zero rather fast and sharply.

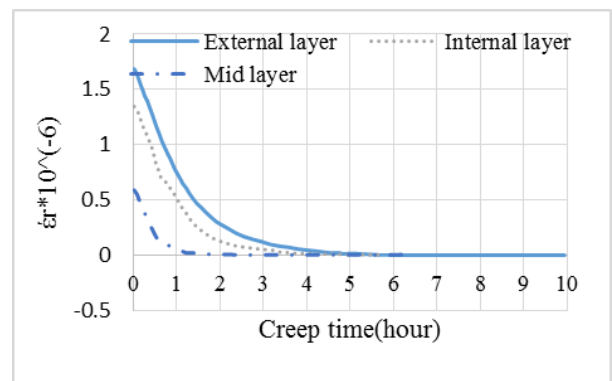


Fig. 12. Radial strain rate distribution curve of creep versus time.

The stress and strain rates, for disc and cylinder made of purposive materials, when creep starts, approach fast from large to small values. This behavior implies that large values of stress and strain rates in the beginning of creep which are considered by some references could not be an appropriate criterion for creep analysis of rotary disc and cylinder.

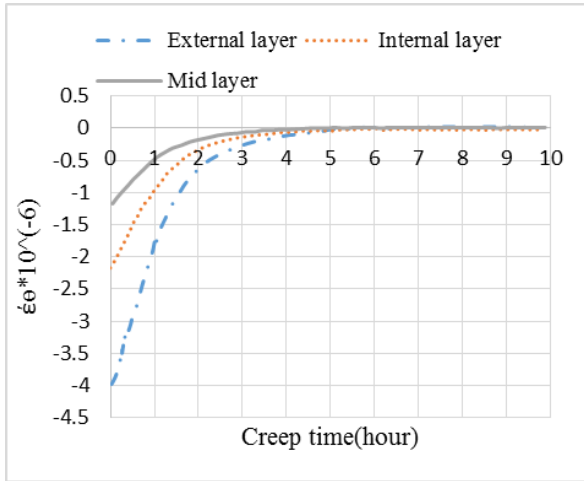


Fig. 13. Tangential strain rate distribution curve of creep versus time.

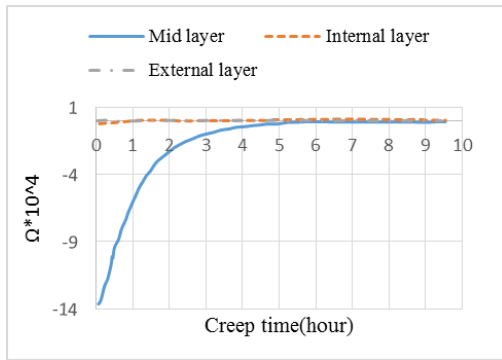


Fig. 14. Radial stress rate distribution curve versus creep time $\Omega = \dot{\sigma}_r$.

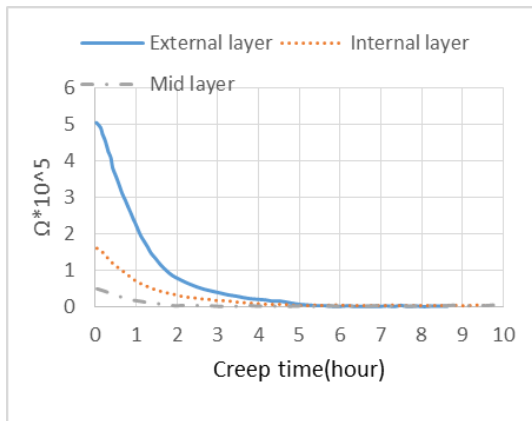


Fig. 15. Tangential stress rate distribution curve versus creep time $\Omega = \dot{\sigma}_t$.

Description of the application of the obtained results:

By increasing dimensionless radius ratio, variation of dimensionless strain for different values of FGM material power and temperature will be converged answers. Increase for different values of FGM material power is reduced ceramic material property and is in-

creased metal properties, as a result, is reduced elasticity modulus and increased strain variations.

4. Conclusions

In the study the following conclusions were drawn:

1. By increasing n , the variation range of related radial strain rises since the increase in n the cylinder properties approach the metal base properties-which has smaller elasticity modulus.
2. By increasing n , radial strain changes from positive values to zero and then to negative values while radial strain values in the middle areas of the cylinder increase in positive direction by n . Also tangential strain will increase in positive direction by growing n .
3. Increasing thermal gradient of the cylinder in areas near the inner surface of the cylinder causes radial strain growth in negative direction. Radial strain decreases in areas near the outer surface, and radial strain increases in the middle areas in positive direction.
4. Increasing thermal gradient causes rise in tangential strain and absolute radial strain rate in the whole cylinder. Notice that this rise in radial strain rate values is not related to linear thermal gradient increases. Also tangential strain rate increases in the whole cylinder in the positive direction by n .
5. The outer and middle layers always (for both strain rates) have maximum and minimum strain rate respectively. Also strain rate approaches zero over creep time that it happens fast.
6. The stress and strain rates, for disc and cylinder made of FGM materials, approach rapidly a steady-state value when creep starts. This behavior implies that large values of stress and strain rates in the beginning of creep which are considered by some references could not be an appropriate criterion for creep analysis of rotary disc and cylinder.
7. Steady-state creep behavior of FGM rotary cylinder strongly depends on the power of variation function. So the power of variation function has an important role in indicating response for design optimization of the cylinder.
8. The FGM rotary cylinder with a power of variation function less than one has a more appropriate creep behavior.
9. The creep strain rates of the FGM rotary cylinder increase sharply by growing thermal gradient. This strong effect of thermal gradient on the

creep behavior of the cylinder indicates the importance of considering exact temperature similar to cylinder working condition in creep behavior analysis of the rotary cylinder.

10. The important effect of considering variable thermodynamic properties of the cylinder in radial direction indicates the necessity for accurate investigation of creep behavior of the rotary cylinder.
11. Different creep behavior of rotary cylinder made of specific materials in different boundary conditions indicates the need to be accurately based on selecting appropriate boundary conditions.

References

- [1] M. Koizumi, Concept of FGM, Ceramic. Trans. 34 (1993) 3-10.
- [2] S.B. Singh, S. Ray, Creep analysis in an isotropic FGM rotating disc of Al-Sic composite, J. Mater. Process. Tech. 143(1) (2003) 616-622.
- [3] S.B. Singh, S. Ray, Modeling the anisotropy and creep in orthotropic aluminum-silicon carbide composite rotating disc, J. Mech. Mater. 34 (2002) 363-372.
- [4] S. Hui-shen, Post buckling analysis of axial loaded functionally graded cylindrical panels in thermal environments. Int. J. Solids. Struct. 39 (2002) 5991-6010.
- [5] L.P. Jacob, Thermoelastic analysis and optimization of functionally graded plates and shells, MSc Thesis, USA: Maine University, 2003.
- [6] K.M. Liew, S. Kitipornchai, X.Z. Zhang, C.W. Lim, Analysis of the thermal stress behavior of functionally graded hollow circular cylinders. Int. J. Solids. Struct. 40 (2003) 2355-2380.
- [7] T. Singh, V.K. Gupta, Effect of anisotropy on steady state creep in functionally graded cylinder, Compos. Struct. 93(2) (2011) 747-758.
- [8] J.F. Durodola, O. Attia, Deformation and stresses in FG rotating disks. Compos. Sci. Technol. 60 (2000) 987-995.
- [9] A. Loghman, V. Atabakhshian, Semi-analytical Solution for Time-dependent creep analysis of rotating cylinders made of anisotropic exponentially graded material (EGM), J. Solid. Mech. 4(3) (2012) 313-326.
- [10] M. Ghannad, G.H. Rahimi, M. Zamani-Nejad, Elastic analysis of pressurized thick cylindrical shells with variable thickness made of functionally graded materials, Composites. 45 (2013) 388-396.
- [11] M. Zamani-Nejad, M.D. Kashkoli, Time-dependent thermo-creep analysis of rotating FGM thick-walled cylindrical pressure vessels under heat ux. Int. J. Eng. Sci. 82 (2014) 222-237.
- [12] M. Zamani-Nejad, M. Jabbari, M. Ghannad, Elastic analysis of FGM rotating thick truncated conical shells with axially-varying properties under non-uniform pressure loading. Compos. Struct. 122 (2015) 561-569.
- [13] M. Zamani-Nejad, M. Jabbari, M. Ghannad, Elastic analysis of axially functionally graded rotating thick cylinder with variable thickness under non-uniform arbitrarily pressure loading. Int. J. Eng. Sci. 89 (2015) 86-99.
- [14] M. Zamani-Nejad, M. Jabbari, M. Ghannad, Elastic analysis of rotating thick cylindrical pressure vessels under non-uniform pressure: Linear and non-linear thickness. Period. Polytech. Mech. 59(2) (2015) 65.
- [15] M. Jabbari, M. Zamani-Nejad, M. Ghannad, Thermoelastic analysis of axially functionally graded rotating thick cylindrical pressure vessels with variable thickness under mechanical loading, Int. J. Eng. Sci. 96 (2015) 1-18.
- [16] A. Loghman, H. Shayeste-moghadam, Magneto-Thermo-Mechanical creep behavior of nanocomposite rotating cylinder made of polypropylene reinforced by MWCNTS, J. Theor. App. Mech-pol. 54 (2011) 239-249.
- [17] M. Garg, B.S. Salaria, V.K. Gupta, Modeling creep in a variable thickness rotating FGM disc under varying thermal gradient, Eng. Computations. 32 (2015) 1230 -1250.
- [18] A. Hassani, M.H. Hojjati, G.H. Farrahi, R.A. Alashti, Semi-exact solution for thermo-mechanical analysis of functionally graded elastic-strain hardening rotating disks. Commun. Nonlinear Sci. Numer. Simul. 17(9) (2012) 3747-3762.
- [19] M. Garg, B.S. Salaria, V.K. Gupta, Effect of disc geometry on the steady-state creep in a rotating disc made of functionally graded material. Mater. Sci. Forum (2013) 183-191.
- [20] K. Khanna, V.K. Gupta, S.P. Nigam, Creep analysis of a variable thickness rotating FGM disc using Tresca Criterion, defence. Sci. J. 65 (2015) 163-170.
- [21] S.A. Hosseini Kordkheili, R. Naghdabadi, Thermoelastic analysis of functionally graded rotating disk, Compos. Struct. 79 (2007) 508-516.